

1 **Particulate biogenic barium tracer of mesopelagic carbon remineralization in the**
2 **Mediterranean Sea (PEACETIME project)**

3

4 Stéphanie H.M. Jacquet^{1*}, Christian Tamburini¹, Marc Garel¹, Aurélie Dufour¹, France
5 VanVambeke¹, Frédéric A.C. Le Moigne¹, Nagib Bhairy¹, Sophie Guasco¹

6

7 ¹Aix Marseille Université, CNRS/INSU, Université de Toulon, IRD, Mediterranean Institute
8 of Oceanography (MIO), UM 110, 13288 Marseille, France

9

10 *Correspondence to: S. Jacquet (stephanie.jacquet@mio.osupytheas.fr)

11

12

13 **PEACETIME special issue**

14

15

16 **ABSTRACT**

17 We report on the sub-basins variability of particulate organic carbon (POC)
18 remineralization in the western and central Mediterranean Sea in late spring during the
19 PEACETIME cruise. POC remineralization rates were estimated using the excess biogenic
20 particulate barium (Ba_{xs}) inventories in the mesopelagic layers (100-1000 m depth) and
21 compared with prokaryotic heterotrophic production (PHP). Ba_{xs} -based mesopelagic
22 remineralization rates (MR) ranged from 25 ± 2 to 306 ± 70 mg C m⁻² d⁻¹. MR were larger in
23 the Algero-Provençal (ALG) basin than in the Tyrrhenian (TYR) and Ionian (ION) basins.
24 Our Ba_{xs} inventories and integrated PHP data also indicated that significant mesopelagic
25 remineralization occurred down to 1000 m depth in the ALG basin in contrast to the ION and
26 TYR basins, where remineralization was mainly located above 500 m depth. We proposed
27 that the higher and deeper MR rates in the ALG basin were sustained by an additional
28 particles export event driven by deep convection. The TYR basin (in contrast to the ALG and
29 ION basins) presented the impact of a previous dust event as reflected by our particulate Al
30 water column concentrations. The ION and TYR basins showed small-scale heterogeneity in
31 remineralization processes, reflected by our Ba_{xs} inventories and integrated PHP data at the
32 #Tyrr long duration station. This heterogeneity was linked to the mosaic of blooming and
33 non-blooming patches reported in this area during the cruise. In contrast to the western
34 Mediterranean Sea (ALG basin), the central Mediterranean Sea (ION and TYR basins)
35 showed lower remineralization rates restricted to the upper mesopelagic layer during the late
36 spring PEACETIME cruise.

37

38 **1. Introduction**

39 In the ocean, remineralization rate associated with sinking particles is a crucial
40 variable for air sea CO₂ balance [Kwon et al., 2009]. Most of the sinking particulate organic
41 carbon (POC) conversion (i.e. remineralization) into CO₂ by heterotrophic organisms (i.e.
42 respiration) occurs within the mesopelagic zone (100-1000 m) [Martin et al., 1987; Buesseler
43 et al., 2007; Buesseler and Boyd, 2009]. A quantitative representation of this process is thus
44 crucial to future predictions of the ocean's role in the global C cycle [IPCC, 2014]. Particulate
45 biogenic barium (Ba_{xs}) is a geochemical tracer of POC remineralization in the mesopelagic
46 layer. Ba_{xs} occurs in the form of barite (BaSO₄ crystals) in the dark ocean as a byproduct of
47 prokaryotic remineralization. In a global ocean undersaturated with respect to barite [Monnin
48 and Cividini, 2006], Ba_{xs} precipitates inside oversaturated biogenic micro-environments
49 during POC degradation by heterotrophic prokaryotes, through sulfate and/or barium
50 enrichment [Dehairs et al., 1980; Stroobant et al., 1991; Bertram and Cowen, 1997;
51 Ganeshram et al., 2003]. By applying a transfer function relating Ba_{xs} to O₂ consumption
52 [Dehairs et al., 1997] Ba_{xs} has been widely used since the 90's as an estimator of mesopelagic
53 POC remineralization rates in various sectors of the Southern Ocean, North Pacific and North
54 Atlantic [Cardinal et al., 2001, 2005; Dehairs et al., 2008; Jacquet et al., 2008a, 2008b, 2011,
55 2015; Planchon et al., 2013; Lemaitre et al., 2018]. Jacquet et al. [2021] recently reported that
56 such transfer function could be applied in the Mediterranean Sea without restriction. This last
57 study complemented previous investigations aiming at improving the use of Ba_{xs} to estimate
58 local processes of POC remineralization in the Mediterranean Sea [Jacquet et al., 2016;
59 Jullion et al., 2017]. The Mediterranean Sea represents a unique case study, mainly due to
60 unresolved issues related to the imbalance in the regional C budget such as the coupling
61 between surface biology and deeper remineralization, timescales of their variability between
62 basins and discrepancies between mesopelagic trophic structure and respiration dynamics

63 [Sternberg et al., 2007, 2008; Santinelli et al., 2010; Lopez-Sandoval et al., 2011; Luna et al.,
64 2012; Tanhua et al., 2013b; Malanotte-Rissoli et al., 2014].

65 The present work is part of the PEACETIME project (ProcEss studies at the Air-sEa
66 Interface after dust deposition in the MEditerranean sea) (<http://peacetime-project.org/>). It
67 aimed at studying the impact of atmospheric Saharan dust on the Mediterranean
68 biogeochemistry [Guieu et al., 2020a]. Dust deposition is a major source of macro and micro
69 nutrients and ballasted material to surface waters that likely impacts the biological carbon
70 pump through organic matter production (i.e. primary production) and its subsequent export
71 and remineralization in the water column [Pabortsava et al., 2017; Gazeau et al., 2021].
72 Overall, the aims of the present contribution to the PEACTIME project were: (1) to document
73 particulate biogenic Ba_{xs} in different ecoregions of the western and central parts of the
74 Mediterranean Sea. Previous Ba_{xs} data in the Mediterranean Sea are relatively scarce with
75 limited vertical sampling resolution [Sanchez-Vidal et al., 2005] or restricted locations
76 [Dehairs et al., 1987; Sternberg et al., 2007, 2008; van Beek et al., 2009]; (2) to determine the
77 relationship between Ba_{xs} and environmental variability, including dust deposition, (3) to
78 estimate Ba_{xs} -based POC remineralization rates (MR) at mesopelagic depths using the
79 Dehairs' transfer function [Dehairs et al., 1997] which we have recently validated for the
80 Mediterranean Sea [Jacquet et al., 2021], and (4) assess potential differences in
81 remineralization length scale of POC in the various ecoregions of the Mediterranean Sea.

82

83 **2. Material and methods**

84 **2.1 Study area**

85 The PEACETIME cruise (<https://doi.org/10.17600/17000300>) was conducted during late
86 spring from May 10 to June 11, 2017 (French R/V Pourquoi pas?) in the western and central
87 Mediterranean (Figure 1a). The Mediterranean Sea is a semi-landlocked sea, with limited but

88 crucial exchange with the Atlantic Ocean, two deep overturning cells, one shallow circulation
89 and a complex upper layer circulation with several permanent and quasi-permanent eddies.

90 The hydrography during the PEACETIME cruise was characterized by three-layers:
91 surface, intermediate and deep waters, typical for the Mediterranean [Tamburini et al., 2013;
92 Tanhua et al., 2013a; Hainbucher et al., 2014, Malanotte-Rizzoli et al., 2014]. Briefly, the
93 main water masses are (see potential temperature – salinity diagram in Figure 1b): (1) from
94 west to east surface Atlantic Water (SW) is gradually replaced by Ionian surface Water (ISW)
95 and Levantine Surface water (LSW); (2) Winter Intermediate Water (WIW) and Levantine
96 Intermediate water (LIW). LIW is present at intermediate depths (from 200 to 800 m) and is
97 characterized by a local maximum of salinity and a local minimum of dissolved oxygen
98 concentration; (4) Mediterranean Deep Water (MDW).

99 Three main ecoregions [Reygondeau et al., 2017; Ayata et al., 2018] were crossed during
100 the cruise: the Algero-Provençal basin (later referred to as ALG), the Tyrrhenian basin (TYR)
101 and the Ionian basin (ION) (Figure 1a). These basins displayed the typical eastward
102 oligotrophic gradient as reported in previous studies [Moutin and Raimbault, 2002; Durrieu
103 de madron et al., 2011; Pujo-Pay et al., 2011; Tanhua et al., 2013a; Reygondeau et al., 2017;
104 Guieu et al., 2020a]. However, this trend was not homogeneous, as for instance in the Ionian
105 Sea (a crossroad of waters of contrasted biological history) where a mosaic of blooming and
106 non-blooming areas co-occurred in spring [Berline et al., 2021]. A diatom-dominated deep
107 chlorophyll maximum that coincided with a maximum in biomass and primary production
108 (PP) was well developed and observed all along the cruise track (Marañón et al., 2021). PP is
109 described in details in Van Wambeke et al. (this issue). Furthermore, important dust
110 deposition affected the TYR basin a few days before our arrival at stations #Tyrr and #5,
111 while in the ALG basin, dust deposition occurred few hours before our sampling at station

112 #Fast (Bressac et al., this issue). POC downward fluxes measured at 200 m depth were similar
113 at the 3 long stations (#Fast, #Tyrr and #Ion).

114

115 **2.2 Barium sampling and sample processing**

116 Thirteen stations were sampled for particulate barium from the surface to 2000 m (thirty
117 depths in total) in the ALG (stations #1, #2, #3, #10, #Fast, #9 and #4), TYR (stations #5,
118 Tyrr and #6) and ION (stations #8, #7 and #Ion) basins (Table 1). Three of these stations were
119 sampled twice on different days (long duration stations #Fast, #Tyrr and #Ion), but due to
120 technical problem no particulate barium data are available for the second visit at station #Ion.
121 Three days separate both visits at station #Fast and two days at #Tyrr.

122 For particulate barium, 4 to 6 L of seawater sampled using Niskin bottles were filtered onto
123 47 mm polycarbonate membranes (0.4 μm porosity) under slight overpressure supplied by
124 filtered air. Filters were rinsed with a few mL of MQ grade water to remove sea salt, dried
125 (50°C) and stored in Petri dishes for later analysis. In the laboratory, we performed a total
126 digestion of filters using a concentrated tri-acid (0.5 mL HF /1.5 mL HNO₃/ HCl 1 mL; all
127 Optima grade) mixture in closed teflon beakers overnight at 95°C in a clean pressurized room.
128 After evaporation close to dryness, samples were re-dissolved into 10 mL of 2% HNO₃.
129 Subsequently, samples were analysed for Ba and other elements of interest (i.e. Al, Na, Sr and
130 Ca) by HR-ICP-MS (High Resolution-Inductively Coupled Plasma- Mass Spectrometry;
131 ELEMENT XR, Thermo). Based on analyses of external certified reference standards,
132 accuracy and reproducibility were both within $\pm 5\%$. More details on sample processing and
133 analysis are given in Cardinal et al. [2001] and Jacquet et al. [2015]. The presence of sea-salt
134 was checked by analysing Na and the sea-salt particulate Ba contribution was found to be
135 negligible ($<0.1\%$ of total Ba). Particulate biogenic barium in excess (hereafter referred to as
136 Ba_{xs}) was calculated as the difference between total Ba and lithogenic Ba. The lithogenic Ba

137 concentration was determined using Al concentration and the upper continental crust (UCC)
138 Ba:Al molar ratio [Dymond et al., 1992; Taylor and Mc Lennan, 1985]. The standard
139 uncertainty [Ellison et al., 2000] on Ba_{xs} concentration ranges between 5.0 and 5.5%. The
140 term “in excess” is used to indicate that concentrations are larger than the Ba_{xs} background
141 (Ba BKG). The background (or residual value) is considered as “preformed” Ba_{xs} at zero
142 oxygen consumption left over after transfer and partial dissolution of Ba_{xs} produced during
143 degradation of previous particles export events. This background Ba_{xs} value likely depends on
144 the saturation state of the water with respect to barite ($BaSO_4$, the main phase of particulate
145 biogenic barium). Saturation indexes were reported in Jacquet et al. [2016] over a high
146 resolution and quasi-zonal Mediterranean transect (M84/3 cruise; Tanhua et al., 2013a,
147 2013b). They revealed that the water column throughout the study area is largely
148 undersaturated, with saturation state ranging between 0.2 and 0.6. A background Ba_{xs} value of
149 130 pM was recently reported in Jacquet et al. [2021]. It is close to the average Ba_{xs} contents
150 observed at greater depth (>1000 m) in the present study (see below).

151

152 **2.3 Prokaryotic heterotrophic production**

153 Prokaryotic heterotrophic production (PHP) estimation was measured by the L-[4,5- 3H]-
154 Leucine (3H -Leu, specific activity 109 Ci mmol⁻¹, PerkinElmer®) incorporation technique
155 (Kirchman, 1993). Details of the protocols can be found in Van Wambeke et al. (2021).
156 Briefly, in epipelagic layers (0-200 m) 1.5 ml seawater samples were incubated at 20 nM 3H -
157 Leu final concentration using the microcentrifuge technique (Smith and Azam, 1992). For the
158 mesopelagic layers, 20 ml (200-800 m depth) and 40 ml (below 800 m depth) seawater
159 samples were incubated using 20 nM and 10 nM 3H -Leu final concentration, respectively,
160 using the filtration technique (Tamburini et al., 2002). Samples were incubated at in situ
161 temperature. To calculate PHP, we used the empirical conversion factor of 1.5 ng C per pmol

162 of incorporated leucine assuming that isotopic dilution was negligible under saturating
163 concentrations of leucine as checked occasionally from concentration kinetics (Van Wambeke
164 et al., 2021).

165

166 **2.4 POC remineralization rates**

167 We recently reported on the validity of the Dehairs's transfer function [Dehairs et al., 1997]
168 in the Mediterranean basin to estimate mesopelagic POC remineralization [Jacquet et al.,
169 2021]. We applied the similar approach to estimate remineralization rates (MR):

$$170 \quad MR = [(Ba_{xs} - Ba_{BKG})/17450] \times Z \times RR \text{ (Eq.1)}$$

171 where Ba_{xs} is the depth-weighted average Ba_{xs} concentration (DWA; pM), i.e. the Ba_{xs}
172 inventory divided by the depth layer considered Z , and RR the Redfield C/O_2 molar ratio
173 (127/175; Broecker et al., 1985). As reported above, a Ba_{BKG} concentration of 130 pM was
174 used. MR rates were then integrated over the 100-500 m (upper mesopelagic zone) and 100-
175 1000 m (entire mesopelagic zone) depth layers.

176

177 **3. Results**

178 Particulate biogenic Ba_{xs} , biogenic Ba fraction (%) and particulate Al, Sr and Ca
179 concentrations are reported in Figure 2 in the upper 2000 m of the water column along a zonal
180 transect crossing the three main sub-basins. PHP rates are also reported in Figure 2 in the
181 upper 500 m along the same transect.

182 Ba_{xs} displayed a similar water column distribution as reported in various sectors of the
183 global Ocean, i.e. relatively low surface concentrations, a maximum in the mesopelagic layer
184 (100-1000 m) followed by a decrease of concentrations back to a background level at deeper
185 depths, usually 1000 m (Figure 3). At stations #9, #Tyrr, #8 and #Ion, Ba_{xs} concentrations in
186 the upper 100 m were quite high (>5000 pM), with values reaching up to 11700 pM at 80 m

187 depth at station #Tyrr (Figure 2a). Such high Ba_{xs} concentrations in the upper layers are quite
188 unusual, though similar values (up to 9000 pM) were occasionally observed in earlier
189 Southern Ocean studies [Dehairs et al., 1991, 1997; Jacquet et al., 2007b, 2008a, 2008b]. The
190 high Ba_{xs} values at stations #Tyrr and #Ion were associated with higher Sr (up to 4267 pM at
191 100 m at station #Ion) and Ca (>130 nM) concentrations (Figure 2d, e). Throughout the water
192 column, Sr and Ca concentrations ranged from 448 to 6938 pM and from 30 to 488 nM,
193 respectively. Sr/Ca molar ratios ranged from 7 to 45 mmol mol⁻¹ within the range of ratios
194 reported in organic material [Martin and Knauer, 1976]. The upper mesopelagic layer (100-
195 500 m) showed the characteristic Ba excess (maximum), as illustrated in Figure 3a. The
196 lithogenic impact on the Ba_{xs} signal was relatively low (<20 %) except at stations #4, #5 and
197 #Tyrr where it reached up to 30 % at some depths in the water column (Figures 2b, 3b). High
198 Ba_{xs} concentrations at stations in the ALG basin and at station #7 in the ION basin extended
199 deeper than at stations in the TYR basin (Figure 2a). At station #Ion Ba_{xs} maximum coincided
200 with higher Ca (up to 186 nM) concentrations in the upper mesopelagic layer (Figure 2e).
201 However, the Ba_{xs} maximum also extended deeper. This is especially salient at stations in the
202 ALG basin. At the other stations Ba_{xs} concentrations below 500 m decreased to reach the
203 background value of around 130 pM. Among stations sampled twice for barium during the
204 cruise, station #Fast (ALG basin) presented similar Ba_{xs} profiles except between 400 and
205 1000 m depth where lower concentrations were measured during the second visit (3 days
206 later; Figure 3a). The Ba_{xs} signal was mostly biogenic and rather stable over the whole water
207 column at this station. This was also the case at station #Ion. In contrast, at station #Tyrr
208 differences between Ba_{xs} profiles mainly occurred in the surface layer and upper mesopelagic
209 layer, with relatively higher Ba_{xs} peaks during the second visit (2 days later; Figure 3b). The
210 biogenic Ba fraction was also more variable throughout the water column at #Tyrr.

211 PHP rates decreased from west to east in surface waters (Figure 2f). At station #Fast,

212 PHP rates decreased from 49 ng C l⁻¹ h⁻¹ in surface to values between 7 and 11 ng C l⁻¹ h⁻¹ at
213 100 m depth and below 6 ng C l⁻¹ h⁻¹ below 200 m depth (Figure 3d). Same trends were found
214 at #Tyrr and #Ion with values in surface waters around 36 and 25 ng C l⁻¹ h⁻¹ respectively
215 (Figures 3e and 3f).

216 Depth-weighted average (DWA) concentrations of Ba_{xs} are reported in Table 1 and
217 Figure 5 for the upper (100-500 m) and entire (100-1000 m) mesopelagic layer. Since the base
218 of the mixed layer was shallower than 100 m, this depth is taken as the upper boundary of the
219 mesopelagic domain. DWA values ranged from 221 to 979 pM. On average, stations located
220 in the ALG basin presented higher DWA than in the TYR and ION basins. DWA Ba_{xs} values
221 remained rather stable over the 3-day period at station #Fast between 100 and 500 m depth,
222 but decreased in deeper layers (Figure 5). As a consequence, the DWA changed from 527 to
223 381 pM for the entire 100-1000 depth layer. In contrast, at station #Tyrr DWA Ba_{xs} values for
224 the 100-500 m and 100-1000 m depth layers increased over the 2-day period (from 284 to
225 542 pM and from 200 to 380 pM, respectively). On average DWA Ba_{xs} reached 577±286,
226 378±123 and 529±213 pM (100-500 m), and 527±288, 280±82 and 358±112 pM (100-1000
227 m) in the ALG, TYR and ION basin, respectively.

228

229 **4. Discussion**

230 **4.1 Ba_{xs} distributions across the sub-basins**

231 The very high Ba_{xs} concentrations reported in the surface layer at stations #9, #Tyrr,
232 #8 and #Ion were associated with local Sr and Ca maxima, likely linked to potentially
233 ballasted phytoplankton-derived material. Similar observations were previously reported in
234 the Southern Ocean, revealing that in the surface water particulate Ba_{xs} is incorporated into or
235 adsorbed onto biogenic material, with barite being a minor component [Dehairs et al., 1991,
236 1997; Jacquet et al., 2007a, 2008a, 2008b]. In deeper layers, Ba_{xs} presented the characteristic

237 maximum reflecting mesopelagic remineralization processes. Mesopelagic Ba_{xs} distributions
238 presented here were similar to those reported in Jacquet et al. [2021] and Sternberg et al.
239 [2008] in the northwestern Mediterranean Sea (ANTARES and DYFAMED observatory sites,
240 respectively). The Ba_{xs} maximum extended down to 1000 m depth in the ALG basin, while it
241 was mostly located in the upper 500 m depth in the TYR basin. The lithogenic impact on the
242 Ba_{xs} signal was relatively very low (<5%), except at stations #4, #5 and #Tyrr where it was
243 more variable and reached up to 30 % at some depths (Figure 2b and 2c). A large dust
244 deposition event occurred over a large area including the southern Tyrrhenian Sea just before
245 the beginning of the PEACETIME campaign. Particulate Al concentrations and estimated
246 lithogenic Ba fraction were sampled at these stations 5 to 12 days after the event and reflected
247 the impact of this dust event in depth. These conclusions are further supported by results
248 reported in Bressac et al. [this issue], showing that Saharan dust depositions strongly
249 impacted Stations #4, #5, #Tyrr and #6 whereby a significant fraction of dust particles was
250 transferred to mesopelagic depths.

251

252 **4.2 Mesopelagic Ba_{xs} and prokaryotic heterotrophic production**

253 Previous studies highlighted the relationship between the mesopelagic Ba_{xs} and the
254 vertical distribution of prokaryotic heterotrophic production (PHP), reflecting the temporal
255 progression of POC remineralization processes. In mesopelagic layers, Ba_{xs} content is smaller
256 when most of the PHP occurs in the upper mixed layer (indicating an efficient, close to
257 complete remineralization within the surface), compared to situations where a significant part
258 of PHP is located deeper in the water column (reflecting significant deep prokaryotic activity
259 and POC export). Figure 3 shows the PHP profiles at long station #Fast, #Tyrr and #Ion (see
260 also VanWambeke et al. [2021] for more detail on PHP). Figure 4 shows the ratio of
261 integrated surface (100 m) to integrated upper mesopelagic (500 m) PHP vs. DWA Ba_{xs}

262 calculated over the 100-500 m depth interval. Results are confronted to the data obtained in
263 the Southern Ocean [Jacquet et al., 2008a, 20015] and recently in the northeast Atlantic and
264 northwestern Mediterranean Sea (PAP and ANTARES observatory sites, respectively)
265 [Jacquet et al., 2021]. The blue line in Figure 4 represents the trend obtained during KEOPS2
266 [Jacquet et al., 2015]; it does not include encircled data points referred to as “season
267 advancement”. Results during PEACETIME followed a similar trend than found for KEOPS2
268 with higher DWA Ba_{xs} in situation where a significant part of column-integrated PHP is
269 located deeper in the water column (high Int.PHP100/Int.PHP500 ratio, Figure 4). Note that
270 some data points, characterized by low DWA Ba_{xs} values, did not follow the trend from
271 KEOPS2 (stations #3, #5 and #Tyrr2). During KEOPS2, the lowest DWA were reported for
272 stations located in a meander and reflecting different (earlier) stages of a bloom compared to
273 the other stations (see “season advancement” in Figure 4). Similarly, station #5 and #Tyrr2
274 reflected the temporal evolution of the establishment (or advanced stages) of mesopelagic
275 remineralization processes in the TYR basin compared to the other basins. Measurements
276 carried out during the second visit at station #Tyrr two days later corroborated this hypothesis
277 showing an increase in remineralization in the upper mesopelagic layer (DWV Ba_{xs} increased
278 from 284 to 542 pM). At the DYFAMED station, Sternberg et al. [2008] reported the seasonal
279 evolution of Ba_{xs} profiles on a monthly basis between February and June 2003. These authors
280 showed the mesopelagic Ba_{xs} build up (and barite stock increase) following the spring
281 phytoplankton bloom development, enhanced POC fluxes and subsequent remineralization.
282 Overall, DWA Ba_{xs} reported in the present study were higher than those reported by
283 Sternberg et al. [2008] (maximum of 463 pM; 0-600 m). The variability over the two days
284 period at station #Tyrr was of the same order of magnitude as the seasonal DWA Ba_{xs}
285 dynamics found at DYFAMED and similar to changes found over a few days to week period
286 in different sectors of the Southern Ocean [Cardinal et al., 2005; Jacquet et al., 2007a; 2015].

287 The column-integrated PHP vs. DWA Ba_{xs} ratio at station #Tyrr confirms that the second
288 occupation experienced higher remineralization rates in the upper mesopelagic layer than
289 during the first one (Table 1).

290

291 **4.3 Mesopelagic C remineralization**

292 POC remineralization rates (MR) estimated from DWA Ba_{xs} values using Eq. (1) are shown
293 in Figure 5 for the upper (100-500 m) and entire (100-1000 m) mesopelagic layer together
294 with primary productivity [van Wambecke et al., 2021]. MR ranged from 25 ± 2 to 306 ± 70
295 $\text{mg C m}^{-2} \text{ d}^{-1}$ and primary production ranged from 138 to $284 \text{ mg C m}^{-2} \text{ d}^{-1}$. Large difference
296 in MR between the upper and the whole mesopelagic layers can be seen in the ALG basin.
297 This is more pronounced at station #9 with MR of $91 \text{ mg C m}^{-2} \text{ d}^{-1}$ in the upper (100 to 500 m
298 depth) layer and $306 \text{ mg C m}^{-2} \text{ d}^{-1}$ in the entire mesopelagic layer (Figure 5). These results
299 show that significant remineralization occurred between 500 and 1000 m in the ALG basin in
300 contrast to the ION and TYR basins where remineralization occurred mainly in the
301 mesopelagic layer between 100 and 500 m depth. Similar conclusion was reached by Jullion
302 et al. [2017] from dissolved Ba and Parametric Optimum Multiparameter (POMP)-derived
303 POC remineralization rates along a zonal transect between the Lebanon coast and Gibraltar
304 (from 156 to $348 \text{ mg C m}^{-2} \text{ d}^{-1}$; M84/3 cruise, April 2011). Independent of any dust input
305 considerations, Jullion et al. [2017] showed significant differences in the mesopelagic MR
306 between the western and eastern Mediterranean, indicating an additional organic carbon
307 export pathway to depth. The western basin is indeed the site of deep shelf and open ocean
308 convection, transferring organic matter to deeper layers [Durrieu de Madron et al., 2013;
309 Stabholz et al., 2013]. The larger MR fluxes found in the ALG basin during PEACETIME are
310 in line with an ecoregion with recurrent injection of material by winter convection (hypothesis
311 of particle injection pump; Boyd et al. [2019]), sustaining higher rates of remineralization

312 below 500 m depth. In contrast in the TYR basin remineralization was mainly located in the
313 upper mesopelagic layer. Stations in the TYR basin received dust inputs a few days before our
314 arrival at these stations; the particulate Al concentrations and estimated lithogenic Ba fraction
315 reflected the impact of this event (Figure 2; Bressac et al., this issue). At station #Tyrr the
316 DAW Ba_{xs} vs. column-integrated PHP increase between the two visits indicated higher MR
317 rates. MR were mainly localized in the upper 500 m. Another atmospheric deposition event
318 occurred on June 5, a few hours after the first sampling at station #Fast in the ALG basin.
319 However, station #Fast does not present any evidence of an impact at mesopelagic depths on
320 particulate Al concentrations and estimated lithogenic Ba. In contrast to conditions in the
321 surface mixed layer, the generation of an observable signal from the mesopelagic
322 remineralization and subsequent Ba_{xs} formation to a single dust event would require more
323 time than the time span between atmospheric deposition and sampling at #Fast (in contrast to
324 station #Tyrr where the dust event occurred 5 to 12 days before). In the ION basin where
325 stations did not reflect the impact of any deposition event and were not subject to potential
326 deep convection, DWA Ba_{xs} and MR fluxes were mostly restricted to the upper mesopelagic
327 layer. Berline et al. [this issue] report small-scale heterogeneity of particles abundances at
328 ION stations, emphasizing the spatial decoupling between particle production and particle
329 distribution and adding complexity in estimating the time lag between production and export
330 of particles, and thus C transfer rate depth [Stange et al., 2017; Henson et al., 2011]. Further,
331 no significant surface production event occurred in the ION basin. However, surface particles
332 at station #8 seemed related to a past production event without significant vertical export by
333 the time the station was sampled. As reported in Van Wambeke et al. [this issue], primary
334 production fluxes were slightly higher in the ION basin (from 158 to 208 mg C m⁻² d⁻¹) than
335 in the TYR basin (from 142 to 170 mg C m⁻² d⁻¹). Overall, DWA Ba_{xs} and MR fluxes reported
336 in the ION basin would thus reflect earlier stage of export and remineralization processes. The

337 same applies to station #Tyrr 2 (in contrast to #Tyrr4) according to the DWA Ba_{xs} vs
338 integrated-PHP trend.

339

340 **5. Conclusion**

341 The present paper expands the data coverage of Ba_{xs} distribution in the ALG, TYR and
342 ION basins (western and central Mediterranean Sea) in late spring 2017. Results highlight that
343 mesopelagic remineralization processes are mainly located in the upper 500 m horizon in the
344 TYR and ION basins, while they occur in the lower mesopelagic zone (down to 1000 m) in
345 the ALG basin. We suggest that particle injection driven by the seasonal winter deep
346 convection in the western basin would sustain the larger and deeper MR rates we observed in
347 the ALG basin. At both TYR and ION basins, Ba_{xs} indicated lower (intensity) and upper
348 mesopelagic-layer restricted remineralization processes that could be the results of a previous
349 dust deposition event (in particular at #Tyrr) or the patchiness of time lags between
350 production and export of particles.

351

352 **Data availability**

353 Guieu et al., Biogeochemical dataset collected during the PEACETIME cruise. SEANOE.
354 <https://doi.org/10.17882/75747> (2020).

355

356 **Author contributions**

357 SJ wrote the manuscript with the contribution of all co-authors. SJ and A. Dufour managed
358 barium analyses; CT, MG, SG and FVV managed PHP analyses. MG, SG and NB performed
359 Ba sampling during the cruise.

360

361 **Competing interests**

362 The authors declare that they have no known competing financial interests or personal
363 relationships that could have appeared to influence the work reported in this paper.

364

365 **Special issue statement**

366 This article is part of the special issue “Atmospheric deposition in the low-nutrient–low-
367 chlorophyll (LNLC) ocean: effects on marine life today and in the future (ACP/BG
368 interjournal SI)”. It is not associated with a conference.

369

370 **Financial Support**

371 The project leading to this publication received funding from CNRS-INSU, IFREMER, CEA,
372 and Météo-France as part of the program MISTRALS coordinated by INSU (doi:
373 10.17600/17000300). The instrument (ELEMENT XR, ThermoFisher) was supported in 2012
374 by European Regional Development Fund (ERDF).

375

376 **Acknowledgments**

377 This study is a contribution to the PEACETIME project (<http://peacetime-project.org>), a
378 joint initiative of the MERMEX and ChArMEx components. PEACETIME was endorsed as a
379 process study by GEOTRACES. It is also a contribution to SOLAS and IMBER. We thank
380 the captain and the crew of the RV Pourquoi Pas? for their professionalism and their work at
381 sea. We warmly thank C. Guieu and K. Deboeufs, as coordinators of the program
382 PEACETIME and chiefs scientists of the campaign. This work is a contribution to the "AT –
383 POMPE BIOLOGIQUE" of the Mediterranean Institute of Oceanography (MIO).

384 **Figures**

385

386 Figure 1: (a) Map of the study area showing the three sub-basins (ALG, TYRR and ION) with
387 stations' locations. The dashed line represents the zonal transect reported in Figure 2; (b)
388 Potential temperature – salinity diagram with isopycnals (kg m^{-3}) for PEACETIME profiles.
389 Graph produced using Ocean Data View (Schlitzer, 2002).

390

391 Figure 2: Sections of (a) particulate biogenic Ba (Ba_{xs} , pM), (c) Al (pM), (d) Sr (pM) and (e)
392 Ca (nM) concentrations, and (b) % biogenic Ba (Ba_{xs}) in the upper 2000 m water column. (f)
393 Section of PHP ($\text{ngC L}^{-1} \text{h}^{-1}$) in the upper 500 m of the water column. Graph produced using
394 Ocean Data View (Schlitzer, 2002).

395

396 Figure 3: (a-c) Ba_{xs} (pM) and (d-f) ($\text{ngC L}^{-1} \text{h}^{-1}$) profiles in the upper 2000 m and 1000 m of
397 the water column, respectively, at long stations #Fast, #Tyrr and #Ion. (a-c) The dashed grey
398 line represents the Ba_{xs} background (BKG) and the grey area represents the fraction for which
399 Ba_{xs} is mostly biogenic.

400

401 Figure 4: Ratio of surface layer integrated PHP (Int.PHPx1) to mesopelagic integrated PHP
402 (Int.PHPx2) versus mesopelagic depth-weighted average (DWA) Ba_{xs} (pM) during
403 PEACETIME. The same data are reported for the KEOPS1 and KEOPS2 cruises (Southern
404 Ocean; Jacquet et al., 2015) and at the PAP (NE-Atlantic) and ANTARES/EMSO-LO (NW-
405 Mediterranean Sea) observatory sites (Jacquet et al., 2021). The blue line ($R^2=0.88$) represents
406 the trend reported during KEOPS2 (Jacquet et al., 2005). The data points referred to as
407 “season advancement” (encircle by the blue line) were excluded from the KEOPS2 regression
408 analysis shown here.

409

410 Figure 5: integrated POC remineralization rates ($\text{mg C m}^{-2} \text{d}^{-1}$) in the upper (100 to 500 m

411 depth) and entire (100 to 1000 m depth) mesopelagic layer in the ALG, TYR and ION basins.

412 Open squares represent primary production ($\text{mg C m}^{-2} \text{d}^{-1}$; Van Wambeke et al., this issue).

413

414

415 **Tables**

416 Table 1: Depth-weighted average (DWA) concentrations of Ba_{xs} (pM) and remineralization
417 rates (MR; $mg\ C\ m^{-2}\ d^{-1}$) for the upper (100 to 500 m depth) and entire (100 to 1000 m depth)
418 mesopelagic layer.

419 **References**

- 420 Ayata, S.-D., Irisson, J.-O., Aubert, A., Berline, L., Dutay, J.-C., Mayot, N., Nieblas, A.-E.,
421 D'Ortenzio, F., Palmiéri, J., Reygondeau, G., Rossi, V., and Guieu, C.: Regionalisation of the
422 Mediterranean basin, a MERMEX synthesis, *Prog. Oceanogr.*, 163, 7–20,
423 <https://doi.org/10.1016/j.pocean.2017.09.016>, 2018.
- 424 van Beek, P., Sternberg, E., Reyss, J.-L., Souhaut, M., Robin, E., and Jeandel, C.:
425 $^{228}\text{Ra}/^{226}\text{Ra}$ and $^{226}\text{Ra}/\text{Ba}$ ratios in the Western Mediterranean Sea: Barite formation and
426 transport in the water column, *Geochim. Cosmochim. Ac.*, 73, 4720–4737,
427 <https://doi.org/10.1016/j.gca.2009.05.063>, 2009.
- 428 Berline, L., Doglioli, A. M., Petrenko, A., Barrillon, S., Espinasse, B., Le Moigne, F. A. C.,
429 Simon-Bot, F., Thyssen, M., and Carlotti, F.: Long distance particle transport to the central
430 Ionian Sea, *Biogeosciences*, 2021, 1–28, <https://doi.org/10.5194/bg-2020-481>, 2021.
- 431 Bertram, M. and P. Cowen, J.: Morphological and compositional evidence for biotic
432 precipitation of marine barite, *J. Mar. Res.*, 55, 577–593, 1997.
- 433 Boyd, P., Claustre, H., Levy, M., Siegel, D., and Weber, T.: Multi-faceted particle pumps
434 drive carbon sequestration in the ocean, *Nature*, 568, 327–335,
435 <https://doi.org/10.1038/s41586-019-1098-2>, 2019.
- 436 Bressac, M., Wagener, T., Leblond, N., Tovar-Sánchez, A., Ridame, C., Albani, S.,
437 Guasco, S., Dufour, A., Jacquet, S., Dulac, F., Desboeufs, K., and Guieu, C.: Subsurface
438 iron accumulation and rapid aluminium removal in the Mediterranean following
439 African dust deposition, *Biogeosciences Discuss.* [preprint],
440 <https://doi.org/10.5194/bg-2021-87>, in review, 2021.
- 441 Broecker, W. S., Takahashi, T., and Takahashi, T.: Sources and flow patterns of deep-ocean
442 waters as deduced from potential temperature, salinity, and initial phosphate concentration, *J.*
443 *Geophys. Res.*, 90, 6925–6939, <https://doi.org/10.1029/JC090iC04p06925>, 1985.

444 Buesseler, K. O. and Boyd, P. W.: Shedding light on processes that control particle export and
445 flux attenuation in the twilight zone of the open ocean, *Limnol. Oceanogr.*, 54, 1210–1232,
446 <https://doi.org/10.4319/lo.2009.54.4.1210>, 2009.

447 Buesseler, K. O., Lamborg, C. H., Boyd, P. W., Lam, P. J., Trull, T. W., Bidigare, R. R.,
448 Bishop, J. K. B., Casciotti, K. L., Dehairs, F., Elskens, M., Honda, M., Karl, D. M., Siegel, D.
449 A., Silver, M. W., Steinberg, D. K., Valdes, J., Van Mooy, B., and Wilson, S.: Revisiting
450 Carbon Flux Through the Ocean's Twilight Zone, *Science*, 316, 567–570,
451 <https://doi.org/10.1126/science.1137959>, 2007.

452 Cardinal, D., Dehairs, F., Cattaldo, T., and André, L.: Geochemistry of suspended particles in
453 the Subantarctic and Polar Frontal zones south of Australia: Constraints on export and
454 advection processes, *J. Geophys. Res.*, 106, 31637–31656,
455 <https://doi.org/10.1029/2000JC000251>, 2001.

456 Cardinal, D., Savoye, N., Trull, T. W., André, L., Kopczynska, E. E., and Dehairs, F.:
457 Variations of carbon remineralisation in the Southern Ocean illustrated by the Baxs proxy,
458 *Deep-Sea Res. Pt. I*, 52, 355–370, <https://doi.org/10.1016/j.dsr.2004.10.002>, 2005.

459 Dehairs, F., Chesselet, R., and Jedwab, J.: Discrete suspended particles of barite and the
460 barium cycle in the open ocean, *Earth. Planet. Sc. Lett.*, 49, 528–550,
461 [https://doi.org/10.1016/0012-821X\(80\)90094-1](https://doi.org/10.1016/0012-821X(80)90094-1), 1980.

462 Dehairs, F., Lambert, C. E., Chesselet, R., and Risler, N.: The biological production of marine
463 suspended barite and the barium cycle in the Western Mediterranean Sea, *Biogeochemistry*, 4,
464 119–140, <https://doi.org/10.1007/BF02180151>, 1987.

465 Dehairs, F., Stroobants, N., and Goeyens, L.: Suspended barite as a tracer of biological
466 activity in the Southern Ocean, *Mar. Chem.*, 35, 399–410, [http://dx.doi.org/10.1016/S0304-](http://dx.doi.org/10.1016/S0304-4203(09)90032-9)
467 [4203\(09\)90032-9](http://dx.doi.org/10.1016/S0304-4203(09)90032-9), 1991.

468 Dehairs, F., Shopova, D., Ober, S., Veth, C., and Goeyens, L.: Particulate barium stocks and
469 oxygen consumption in the Southern Ocean mesopelagic water column during spring and
470 early summer: relationship with export production, *Deep-Sea Res. Pt. II*, 44, 497–516,
471 [https://doi.org/10.1016/S0967-0645\(96\)00072-0](https://doi.org/10.1016/S0967-0645(96)00072-0), 1997.

472 Dehairs, F., Jacquet, S., Savoye, N., Van Mooy, B. A. S., Buesseler, K. O., Bishop, J. K. B.,
473 Lamborg, C. H., Elskens, M., Baeyens, W., Boyd, P. W., Casciotti, K. L., and Monnin, C.:
474 Barium in twilight zone suspended matter as a potential proxy for particulate organic carbon
475 remineralization: Results for the North Pacific, *Deep-Sea Res. Pt. II*, 55, 1673–1683,
476 <https://doi.org/10.1016/j.dsr2.2008.04.020>, 2008.

477 Durrieu de Madron, X., Guieu, C., Sempéré, R., Conan, P., Cossa, D., D’Ortenzio, F.,
478 Estournel, C., Gazeau, F., Rabouille, C., Stemmann, L., Bonnet, S., Diaz, F., Koubbi, P.,
479 Radakovitch, O., Babin, M., Baklouti, M., Bancon-Montigny, C., Belviso, S., Bensoussan, N.,
480 Bonsang, B., Bouloubassi, I., Brunet, C., Cadiou, J.-F., Carlotti, F., Chami, M., Charmasson,
481 S., Charrière, B., Dachs, J., Doxaran, D., Dutay, J.-C., Elbaz-Poulichet, F., Eléaume, M.,
482 Eyrolles, F., Fernandez, C., Fowler, S., Francour, P., Gaertner, J. C., Galzin, R., Gasparini, S.,
483 Ghiglione, J.-F., Gonzalez, J.-L., Goyet, C., Guidi, L., Guizien, K., Heimbürger, L.-E.,
484 Jacquet, S. H. M., Jeffrey, W. H., Joux, F., Le Hir, P., Leblanc, K., Lefèvre, D., Lejeusne, C.,
485 Lemé, R., Loÿe-Pilot, M.-D., Mallet, M., Méjanelle, L., Mélin, F., Mellon, C., Mérigot, B.,
486 Merle, P.-L., Migon, C., Miller, W. L., Mortier, L., Mostajir, B., Mousseau, L., Moutin, T.,
487 Para, J., Pérez, T., Petrenko, A., Poggiale, J.-C., Prieur, L., Pujo-Pay, M., Pulido-Villena,
488 Raimbault, P., Rees, A. P., Ridame, C., Rontani, J.-F., Ruiz Pino, D., Sicre, M. A.,
489 Taillandier, V., Tamburini, C., Tanaka, T., Taupier-Letage, I., Tedetti, M., Testor, P.,
490 Thébault, H., Thouvenin, B., Touratier, F., Tronczynski, J., Ulses, C., Van Wambeke, F.,
491 Vantrepotte, V., Vaz, S., and Verney, R.: Marine ecosystems’ responses to climatic and

492 anthropogenic forcings in the Mediterranean, *Prog. Oceanogr.*, 91, 97–166,
493 <https://doi.org/10.1016/j.pocean.2011.02.003>, 2011.

494 Dymond, J. R., Suess, E., and Lyle, M.: Barium in deep-sea sediment: a geochemical proxy
495 for paleoproductivity, *Paleoceanography*, 7, 163–181, 1992.

496 Ellison, S. L. R.: Eurachem/CITAC Guide CG4, Quantifying Uncertainty in Analytical
497 Measurement, 2nd Edn., edited by: Ellison, S. L. R., Rosslein, M., and Williams, A., 120 pp.,
498 ISBN 0948926 15 5, 2000.

499 Ganeshram, R. S., François, R., Commeau, J., and Brown-Leger, S. L.: An experimental
500 investigation of barite formation in seawater, *Geochim. Cosmochim. Ac.*, 67, 2599–2605,
501 [https://doi.org/10.1016/S0016-7037\(03\)00164-9](https://doi.org/10.1016/S0016-7037(03)00164-9), 2003.

502 Gazeau, F., Van Wambeke, F., Marañon, E., Pérez-Lorenzo, M., Alliouane, S., Stolpe, C.,
503 Blasco, T., Leblond, N., Zäncker B., Engel A., Marie, B., Dinasquet, J., and Guieu C.: Impact
504 of dust addition on the metabolism of Mediterranean plankton communities and carbon export
505 under present and future conditions of pH and temperature, *Biogeosciences Discuss.*
506 [preprint], <https://doi.org/10.5194/bg-2021-20>, in review, 2021.

507 Guieu, C., D’Ortenzio, F., Dulac, F., Taillandier, V., Doglioli, A., Petrenko, A., Barrillon, S.,
508 Mallet, M., Nabat, P., and Desboeufs, K.: Introduction: Process studies at the air–sea interface
509 after atmospheric deposition in the Mediterranean Sea – objectives and strategy of the
510 PEACETIME oceanographic campaign (May–June 2017), *Biogeosciences*, 17, 5563–5585,
511 <https://doi.org/10.5194/bg-17-5563-2020>, 2020a.

512 Guieu, C., and Desboeufs, K. : PEACETIME cruise, RV Pourquoi pas?,
513 <https://doi.org/10.17600/17000300>, 2017.

514 Guieu, C., Desboeufs, K., Albani, S., et al.: Biogeochemical dataset collected during the
515 PEACETIME cruise, available at: <https://www.seanoe.org/data/00645/75747/>, 2020b.

516 Hainbucher, D., Rubino, A., Cardin, V., Tanhua, T., Schroeder, K., and Bensi, M.:
517 Hydrographic situation during cruise M84/3 and P414 (spring 2011) in the Mediterranean
518 Sea, *Ocean Sci.*, 10, 669–682, <https://doi.org/10.5194/os-10-669-2014>, 2014.

519 Henson, S. A., Sanders, R., Madsen, E., Morris, P. J., Le Moigne, F., and Quartly, G. D.: A
520 reduced estimate of the strength of the ocean’s biological carbon pump, *Geophys. Res. Lett.*,
521 38, L04606, <https://doi.org/10.1029/2011GL046735>, 2011.

522 IPCC: 5th Assessment Report (AR5) Climate Change 2013, Working Group 1, January 2014.

523 Jacquet, S. H. M., Dehairs, F., Elskens, M., Savoye, N., and Cardinal, D.: Barium cycling
524 along WOCE SR3 line in the Southern Ocean, *Mar. Chem.*, 106, 33–45,
525 <https://doi.org/10.1016/j.marchem.2006.06.007>, 2007a.

526 Jacquet, S. H. M., Henjes, J., Dehairs, F., Worobiec, A., Savoye, N., and Cardinal, D.:
527 Particulate Ba-barite and acantharians in the Southern Ocean during the European Iron
528 Fertilization Experiment (EIFEX), *J. Geophys. Res.*, 112,
529 <https://doi.org/10.1029/2006JG000394>, 2007b.

530 Jacquet, S. H. M., Savoye, N., Dehairs, F., Strass, V. H., and Cardinal, D.: Mesopelagic
531 carbon remineralization during the European Iron Fertilization Experiment, *Global*
532 *Biogeochem. Cycles*, 22, GB1023, <https://doi.org/10.1029/2006GB002902>, 2008a.

533 Jacquet, S. H. M., Dehairs, F., Savoye, N., Obernosterer, I., Christaki, U., Monnin, C., and
534 Cardinal, D.: Mesopelagic organic carbon remineralization in the Kerguelen Plateau region
535 tracked by biogenic particulate Ba, *Deep-Sea Res. Pt. II*, 55, 868–879,
536 <https://doi.org/10.1016/j.dsr2.2007.12.038>, 2008b.

537 Jacquet, S. H. M., Dehairs, F., Dumont, I., Becquevort, S., Cavagna, A.-J., and Cardinal, D.:
538 Twilight zone organic carbon remineralization in the Polar Front Zone and Subantarctic Zone
539 south of Tasmania, *Deep-Sea Res. Pt. II*, 58, 2222–2234,
540 <https://doi.org/10.1016/j.dsr2.2011.05.029>, 2011.

541 Jacquet, S. H. M., Dehairs, F., Lefèvre, D., Cavagna, A. J., Planchon, F., Christaki, U.,
542 Monin, L., André, L., Closset, I., and Cardinal, D.: Early spring mesopelagic carbon
543 remineralization and transfer efficiency in the naturally iron-fertilized Kerguelen area,
544 *Biogeosciences*, 12, 1713–1731, <https://doi.org/10.5194/bg-12-1713-2015>, 2015.

545 Jacquet, S. H. M., Monnin, C., Riou, V., Jullion, L., and Tanhua, T.: A high resolution and
546 quasi-zonal transect of dissolved Ba in the Mediterranean Sea, *Mar. Chem.*, 178, 1–7,
547 <https://doi.org/10.1016/j.marchem.2015.12.001>, 2016.

548 Jacquet, S. H. M., Lefèvre, D., Tamburini, C., Garel, M., Le Moigne, F. A. C., Bhairy, N., and
549 Guasco, S.: On the barium–oxygen consumption relationship in the Mediterranean Sea:
550 implications for mesopelagic marine snow remineralization, *Biogeosciences*, 18, 2205–2212,
551 <https://doi.org/10.5194/bg-18-2205-2021>, 2021.

552 Jullion, L., Jacquet, S. H. M., and Tanhua, T.: Untangling biogeochemical processes from the
553 impact of ocean circulation: First insight on the Mediterranean dissolved barium dynamics,
554 *Global Biogeochem. Cycles*, 31, 1256–1270, <https://doi.org/10.1002/2016GB005489>, 2017.

555 Kirchman, D. L.: Leucine incorporation as a measure of biomass production by heterotrophic
556 bacteria, in: *Handbooks of methods in aquatic microbial ecology*, edited by: Kemp, P. F.,
557 Sherr, B. F., Sherr, E. B., and Cole, J. J., Lewis Publishers, Boca Raton, Ann Arbor, London,
558 Tokyo, 509–512, 1993.

559 Kwon, E. Y., Primeau, F., and Sarmiento, J. L.: The impact of remineralization depth on the
560 air–sea carbon balance, *Nat. Geosci.*, 2, 630–635, <https://doi.org/10.1038/ngeo612>, 2009.

561 Lemaitre, N., Planquette, H., Planchon, F., Sarthou, G., Jacquet, S., García-Ibáñez, M. I.,
562 Gourain, A., Cheize, M., Monin, L., André, L., Laha, P., Terryn, H., and Dehairs, F.:
563 Particulate barium tracing of significant mesopelagic carbon remineralisation in the North
564 Atlantic, *Biogeosciences*, 15, 2289–2307, <https://doi.org/10.5194/bg-15-2289-2018>, 2018.

565 López-Sandoval, D. C., Fernández, A., and Marañón, E.: Dissolved and particulate primary
566 production along a longitudinal gradient in the Mediterranean Sea, *Biogeosciences*, 8, 815–
567 825, <https://doi.org/10.5194/bg-8-815-2011>, 2011.

568 Luna, G. M., Bianchelli, S., Decembrini, F., De Domenico, E., Danovaro, R., and Dell’Anno,
569 A.: The dark portion of the Mediterranean Sea is a bioreactor of organic matter cycling,
570 *Global Biogeochem. Cycles*, 26, GB2017, <https://doi.org/10.1029/2011GB004168>, 2012.

571 Malanotte-Rizzoli, P., Artale, V., Borzelli-Eusebi, G. L., Brenner, S., Crise, A., Gacic, M.,
572 Kress, N., Marullo, S., Ribera d’Alcalà, M., Sofianos, S., Tanhua, T., Theocharis, A., Alvarez,
573 M., Ashkenazy, Y., Bergamasco, A., Cardin, V., Carniel, S., Civitarese, G., D’Ortenzio, F.,
574 Font, J., Garcia-Ladona, E., Garcia-Lafuente, J. M., Gogou, A., Gregoire, M., Hainbucher, D.,
575 Kontoyannis, H., Kovacevic, V., Kraskapoulou, E., Kroskos, G., Incarbona, A., Mazzocchi,
576 M. G., Orlic, M., Ozsoy, E., Pascual, A., Poulain, P.-M., Roether, W., Rubino, A., Schroeder,
577 K., Siokou-Frangou, J., Souvermezoglou, E., Sprovieri, M., Tintoré, J., and Triantafyllou, G.:
578 Physical forcing and physical/biochemical variability of the Mediterranean Sea: a review of
579 unresolved issues and directions for future research, *Ocean Sci.*, 10, 281–322,
580 <https://doi.org/10.5194/os-10-281-2014>, 2014.

581 Martin, J. H., and G. A. Knauer (1973), Elemental composition of plankton, *Geochim.*
582 *Cosmochim. Acta*, 37(7), 1639– 1653.

583 Martin, J. H., Knauer, G. A., Karl, D. M., and Broenkow, W. W.: VERTEX: carbon cycling
584 in the northeast Pacific, *Deep-Sea Res.*, 34, 267–285, [http://dx.doi.org/10.1016/0198-](http://dx.doi.org/10.1016/0198-0149(87)90086-0)
585 [0149\(87\)90086-0](http://dx.doi.org/10.1016/0198-0149(87)90086-0), 1987.

586 Monnin, C. and Cividini, D.: The saturation state of the world’s ocean with respect to
587 (Ba,Sr)SO₄ solid solutions, *Geochim. Cosmochim. Ac.*, 70, 3290–3298,
588 <https://doi.org/10.1016/j.gca.2006.04.002>, 2006.

589 Moutin, T. and Raimbault, P.: Primary production, carbon export and nutrients availability in
590 western and eastern Mediterranean Sea in early summer 1996 (MINOS cruise), *J. Marine*
591 *Syst.*, 33–34, 273–288, [https://doi.org/10.1016/S0924-7963\(02\)00062-3](https://doi.org/10.1016/S0924-7963(02)00062-3), 2002.

592 Pabortsava, K., Lampitt, R. S., Benson, J., Crowe, C., McLachlan, R., Le Moigne, F. A. C.,
593 Mark Moore, C., Pebody, C., Provost, P., Rees, A. P., Tilstone, G. H., and Woodward, E. M.
594 S.: Carbon sequestration in the deep Atlantic enhanced by Saharan dust, *Nature Geoscience*,
595 10, 189–194, <https://doi.org/10.1038/ngeo2899>, 2017.

596 Planchon, F., Cavagna, A.-J., Cardinal, D., André, L., and Dehairs, F.: Late summer
597 particulate organic carbon export and twilight zone remineralisation in the Atlantic sector of
598 the Southern Ocean, *Biogeosciences*, 10, 803–820, <https://doi.org/10.5194/bg-10-803-2013>,
599 2013.

600 Pujo-Pay, M., Conan, P., Oriol, L., Cornet-Barthaux, V., Falco, C., Ghiglione, J.-F., Goyet,
601 C., Moutin, T., and Prieur, L.: Integrated survey of elemental stoichiometry (C, N, P) from the
602 western to eastern Mediterranean Sea, *Biogeosciences*, 8, 883–899,
603 <https://doi.org/10.5194/bg-8-883-2011>, 2011.

604 Reygondeau, G., Guieu, C., Benedetti, F., Irisson, J.-O., Ayata, S.-D., Gasparini, S., and
605 Koubbi, P.: Biogeochemical regions of the Mediterranean Sea: An objective multidimensional
606 and multivariate environmental approach, *Prog. Oceanogr.*, 151, 138–148,
607 <http://dx.doi.org/10.1016/j.pocean.2016.11.001>, 2017.

608 Sanchez-Vidal, A., Collier, R. W., Calafat, A., Fabres, J., and Canals, M.: Particulate barium
609 fluxes on the continental margin: a study from the Alboran Sea (Western Mediterranean),
610 *Mar. Chem.*, 93, 105–117, <https://doi.org/10.1016/j.marchem.2004.07.004>, 2005.

611 Santinelli, C., Nannicini, L., and Seritti, A.: DOC dynamics in the meso and bathypelagic
612 layers of the Mediterranean Sea, *Deep-Sea Res. Pt. II*, 57, 1446–1459,
613 <https://doi.org/10.1016/j.dsr2.2010.02.014>, 2010.

614 Schlitzer, R.: Ocean Data View, GEO/ODV, available at: <http://www.awi-bremerhaven.de/>
615 (last access: 2 March 2021), 2002.

616 Simon, M. and Azam, F.: Protein content and protein synthesis rates of planktonic marine
617 bacteria, *Mar. Ecol. Prog. Ser.*, 51, 201–213, 1989.

618 Stabholz, M., Durrieu de Madron, X., Canals, M., Khripounoff, A., Taupier-Letage, I., Testor,
619 P., Heussner, S., Kerhervé, P., Delsaut, N., Houpert, L., Lastras, G., and Dennielou, B.:
620 Impact of open-ocean convection on particle fluxes and sediment dynamics in the deep
621 margin of the Gulf of Lions, *Biogeosciences*, 10, 1097–1116, [https://doi.org/10.5194/bg-10-](https://doi.org/10.5194/bg-10-1097-2013)
622 [1097-2013](https://doi.org/10.5194/bg-10-1097-2013), 2013.

623 Stange, P., Bach, L. T., Le Moigne, F. A. C., Taucher, J., Boxhammer, T., and Riebesell, U.:
624 Quantifying the time lag between organic matter production and export in the surface ocean:
625 Implications for estimates of export efficiency, *Geophys. Res. Lett.*, 44, 268–276,
626 <https://doi.org/10.1002/2016GL070875>, 2017.

627 Sternberg, E., Jeandel, C., Miquel, J.-C., Gasser, B., Souhaut, M., Arraes-Mescoff, R., and
628 Francois, R.: Particulate barium fluxes and export production in the northwestern
629 Mediterranean, *Mar. Chem.*, 105, 281–295, <https://doi.org/10.1016/j.marchem.2007.03.003>,
630 2007.

631 Sternberg, E., Jeandel, C., Robin, E., and Souhaut, M.: Seasonal cycle of suspended barite in
632 the mediterranean sea, *Geochim. Cosmochim. Ac.*, 72, 4020–4034,
633 <https://doi.org/10.1016/j.gca.2008.05.043>, 2008.

634 Stroobants, N., Dehairs, F., Goeyens, L., Vanderheijden, N., and Van Grieken, R.: Barite
635 formation in the Southern Ocean water column, *Mar. Chem.*, 35, 411–421,
636 [https://doi.org/10.1016/S0304-4203\(09\)90033-0](https://doi.org/10.1016/S0304-4203(09)90033-0), 1991.

637 Tamburini, C., Garcin, J., Ragot, M., and Bianchi, A.: Biopolymer hydrolysis and bacterial
638 production under ambient hydrostatic pressure through a 2000m water column in the NW

639 Mediterranean, *Deep-Sea Res. Pt. I*, 49, 2109–2123, <https://doi.org/10.1016/S0967->
640 [0645\(02\)00030-9](https://doi.org/10.1016/S0967-0645(02)00030-9), 2002.

641 Tamburini, C., Boutrif, M., Garel, M., Colwell, R. R., and Deming, J. W.: Prokaryotic
642 responses to hydrostatic pressure in the ocean – a review, *Environ. Microbiol.*, 15, 1262–
643 1274, <https://doi.org/10.1111/1462-2920.12084>, 2013.

644 Tanhua, T., Hainbucher, D., Cardin, V., Álvarez, M., Civitarese, G., McNichol, A. P., and
645 Key, R. M.: Repeat hydrography in the Mediterranean Sea, data from the
646 <i>Meteor</i> cruise 84/3 in 2011, *Earth Syst. Sci. Data*, 5, 289–294,
647 <https://doi.org/10.5194/essd-5-289-2013>, 2013a.

648 Tanhua, T., Hainbucher, D., Schroeder, K., Cardin, V., Álvarez, M., and Civitarese, G.: The
649 Mediterranean Sea system: a review and an introduction to the special issue, *Ocean Sci.*, 9,
650 789–803, <https://doi.org/10.5194/os-9-789-2013>, 2013b.

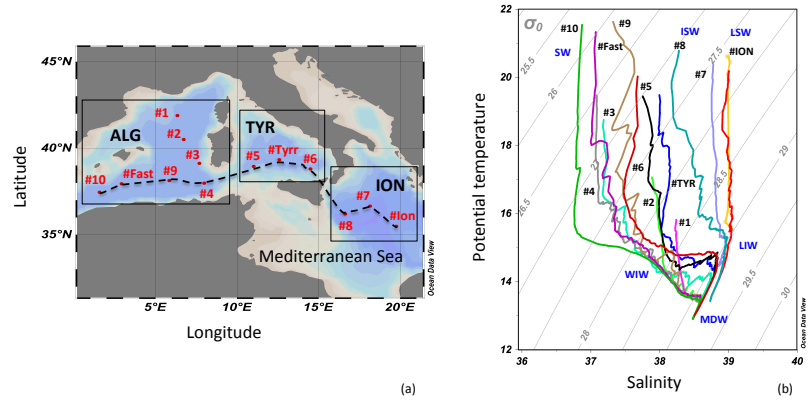
651 Taylor, S. R. and McLennan, S. M.: *The continental crust: its composition and evolution*,
652 Blackwell Scientific Publications, USA, 312 pp., 1985.

653 Van Wambeke, F., Taillandier, V., Deboeufs, K., Pulido-Villena, E., Dinasquet, J., Engel, A.,
654 Marañón, E., Ridame, C., and Guieu, C.: Influence of atmospheric deposition on
655 biogeochemical cycles in an oligotrophic ocean system, *Biogeosciences*, 2020, 1–51,
656 <https://doi.org/10.5194/bg-2020-411>, 2020.

657
658
659
660
661
662
663
664

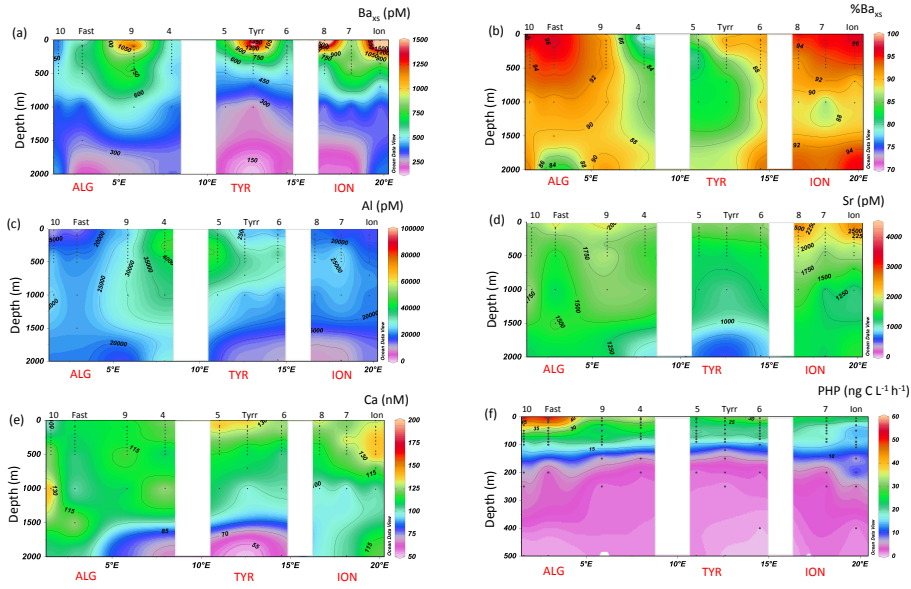
665
666
667
668
669
670
671
672
673
674
675
676

Figure 1



677
678
679
680
681
682

Figure 2

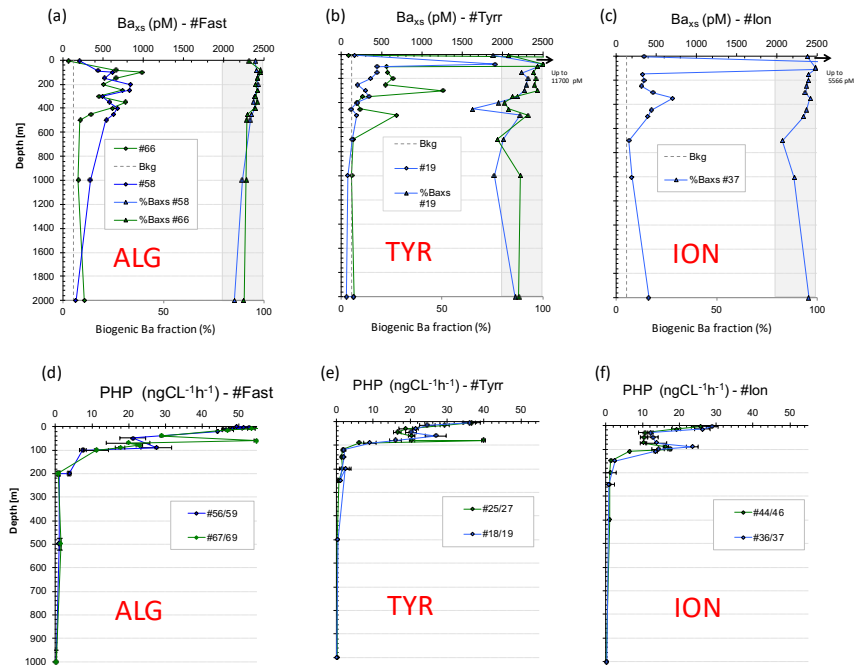


683

684

685

686 Figure 3

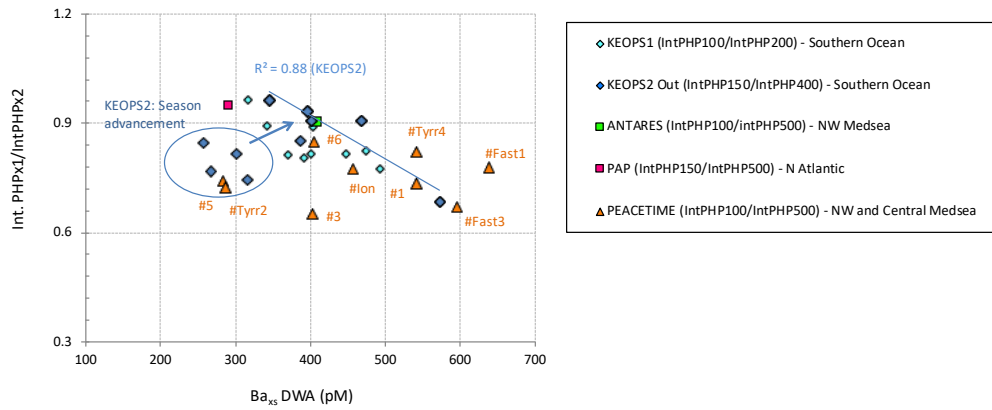


687

688

689

690 Figure 4



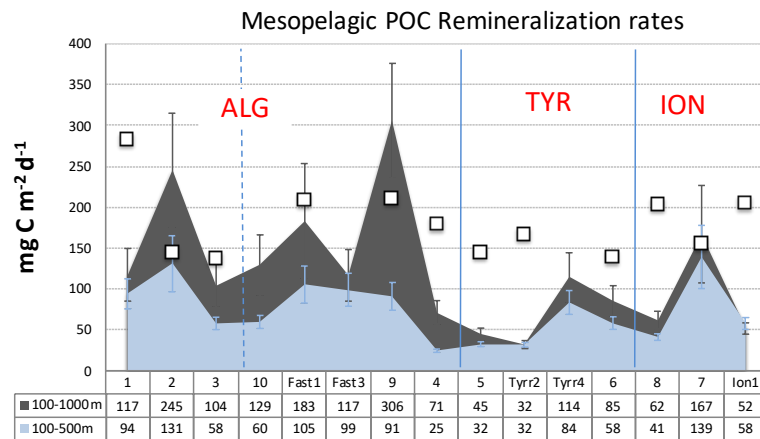
691

692

693

694

695 Figure 5



696

697

698

699 Table 1

Basin	Station #	Mesopelagic layer	DWA Ba _{xs} [pM]	MR [mg C m ⁻² d ⁻¹]	MR Stnd error [%]
Algero-Provençal	1	upper	542	94	20
	1	entire	374	117	27
	2	upper	717	131	26
	2	entire	645	245	28
	3	upper	402	58	13
	3	entire	353	104	25
	4	upper	243	25	8
	4	entire	281	71	20
	9	upper	981	91	19
	9	entire	979	306	23
	Fast1	upper	638	105	21
	Fast1	entire	527	183	38
	Fast3	upper	596	99	20
	Fast3	entire	381	117	27
	10	upper	418	60	13
	10	entire	410	129	29
Tyrrhenian	5	upper	283	32	9
	5	entire	226	45	17
	Tyrr2	upper	284	32	9
	Tyrr2	entire	200	32	15
	Tyrr4	upper	542	84	17
	Tyrr4	entire	380	114	26
	6	upper	404	58	13
	6	entire	313	85	22
Ionian	7	upper	769	139	28
	7	entire	485	167	36
	ION	upper	456	58	13
	ION	entire	315	52	13
	8	upper	363	41	10
	8	entire	273	62	18

700